Partial-MIMO Based Mode-Group Transmission and Routing in a Field-Deployed 15-Mode Network: Throughput, DSP Resources and Network Flexibility

Alberto Gatto, *Member, IEEE*, Paola Parolari, *Senior Member, IEEE*, Ruben S. Luis, *Senior Member, IEEE*, Georg Rademacher, *Senior Member, IEEE*, Benjamin J. Puttnam, *Member, IEEE*, Robert Emmerich, Colja Schubert, Giuseppe Ferri, *Senior Member, IEEE*, Frank Achten, Pierre Sillard, *Member, IEEE*, Paolo Martelli, *Member, IEEE*, Giammarco Di Sciullo, Andrea Marotta, *Member, IEEE*, Antonio Mecozzi, *Fellow, IEEE*, Cristian Antonelli, *Senior Member, IEEE*, and Pierpaolo Boffi, *Senior Member, IEEE*

***Abstract*—Transmission based on mode-division multiplexing can enhance node flexibility in metropolitan networks by exploiting mode-group routing. In fact, each mode group, constituted by degenerate spatial modes, can act as a single modal super-channel: since the inter-group crosstalk remains limited or even negligible among different mode groups for sufficiently short distances, typical of urban scenarios, the mode groups can be optically multiplexed and demultiplexed at the network nodes. Moreover, each group can cover an optical path independent from the propagation of the other groups, and be received by means of a so-called partial-MIMO processing, handling just its own degenerate modes, with a significant reduction of the necessary digital resources. In this paper we experimentally assess the capabilities of such a mode-group approach using a few-mode fiber, supporting 5 mode groups, already deployed in the city of L'Aquila, Italy. Transmission throughput versus DSP resources (in terms of number of taps required to achieve a proper GMI) is analyzed, experimenting different modulation formats (at 50 Gbaud), in case of 75-GHz spaced WDM transmission. The large number of spatial modes supported by the few-mode fiber employed in the field-trial allows to explore several combinations of transmitted mode groups in order to better understand how the inter-group cross-talk affects the capacity performance. Almost 2-Tb/s capacity per WDM channel is demonstrated for 6 WDM channels over 6.1-km few-mode fiber reach, thanks to partial MIMO. Finally, multi-hop routing is also performed in a 4-node scenario, in particular taking into account the impact of the optical mode multiplexer/demultiplexer employed in the field trial on the routed throughput per wavelength.**

***Index Terms*—Few mode fibers, MIMO processing, mode group division multiplexing.**

Manuscript received 21 November 2023; revised 29 February 2024; accepted 27 March 2024. Date of publication 29 March 2024; date of current version 16 July 2024. This work was supported in part by Italian Government through the MUR PRIN2017 "FIRST" Project under Grant GA 2017HP5KH7_002 and INCIPICT Project, in part by the German Federal Ministry of Education and Research (BMBF) under Grant 16KIS1419 (STARFALL), in part by CELTIC EUREKA Project AI-NET- PROTECT under Grant C2019/3-4, and in part by the BMBF Contract under Grant 16KIS1282. *(Corresponding author: Alberto Gatto.)*

Alberto Gatto, Paola Parolari, Paolo Martelli, and Pierpaolo Boffi are with the Department of Electronics, Information and Bioengineering, Politecnico di Milano, 20133 Milano, Italy (e-mail: alberto.gatto@polimi.it).

Ruben S. Luis and Benjamin J. Puttnam are with the National Institute of Information and Communication Technology (NICT), Tokyo 184-8795, Japan.

Georg Rademacher is with the University of Stuttgart, 70174 Stuttgart, Germany.

Robert Emmerich and Colja Schubert are with the Fraunhofer Institute for Telecommunications, Heinrich-Hertz-Institute, 10587 Berlin, Germany.

Giuseppe Ferri, Frank Achten, and Pierre Sillard are with Prysmian Group, 20126 Milano, Italy.

Giammarco Di Sciullo, Andrea Marotta, Antonio Mecozzi, and Cristian Antonelli are with the University of L'Aquila and CNIT, 67100 L'Aquila, Italy.

Color versions of one or more figures in this article are available at https://doi.org/10.1109/JLT.2024.3383290.

Digital Object Identifier 10.1109/JLT.2024.3383290

I. Introduction

MODE division multiplexing (MDM) is a well-known technique to increase the capacity transported on a single link through the exploitation of multi-mode fibers (MMF) or few-mode fibers (FMFs) [1]. The total transmitted capacity can be multiplied by a factor approaching the number of spatial modes supported by the MMF/ FMF, using coherent detection at the receiver side. To contain the detrimental effects of inter-modal crosstalk (IMXT) [2], [3], which represents the main impairment impacting on MDM performance, massive multiple input multiple output (MIMO) processing is normally employed. However, the requested MIMO processing may be prohibitive for short-reach, and cost-limited applications, which may favor transmissions over fibers able to support uncoupled spatial channels, e.g. multicore fibers (MCFs) [4]. Moreover, MIMO application requires that all the spatial modes cover the same physical path to be processed together after coherent detection [5], thus permitting just point-to-point connections. The flexibility of the optical network is reduced, as all the used spatial modes must be accessible at each network node, in order to allow a potential full-MIMO processing, even if the spatial channels contain services with different final destinations [6]. A possible solution could be the use of partial-MIMO processing on degenerate modes [7], [8], which permits to reduce the system complexity and the multiplexing and switching of several independent channels as long as the IMXT is limited.

An alternative approach is mode-group division multiplexing (MGDM) [9], where the spatial modes of the same mode group (MG), strongly coupled, constitute a single modal

super-channel. MGDM could represent a suitable solution for metropolitan networks, considering that the inter-group crosstalk (IGXT) remains limited or even negligible among different MGs for sufficiently short distances [10]. In such a scheme, the transmission is performed only within specific MGs that are distant enough to neglect or tolerate the IGXT [11]. In this case, the partial MIMO processing at the receiver side can be applied to each transmitted MG separately, to recover just the degenerate modes belonging to the same MG, thus yielding to a substantial reduction of the required resources. Moreover, this solution allows also routing applications over short and medium reach scenarios [10], [12], where the IGXT is low or even negligible. The different MGs, in fact, can be handled independently, improving the granularity in switching and enabling multi-hop routing in both spectrum and space dimensions.

Recently, MGDM transmission has been demonstrated in OM2 multimode fibers to achieve > 1 Tb/s capacity, exploiting conventional wavelength division multiplexing (WDM), discrete multitone (DMT) modulation and direct detection [13], [14]. Moreover, the MIMO-free configuration has been proposed in [15], based on the selective excitation of a single channel per mode group and coherent detection in a 15-mode FMF. In this case, the achievable total capacity is proportional to the number of the excited MGs, and not to the total number of the co-propagating spatial modes. This solution permits to increase the capacity transported on a single link, avoiding the employment of power-hungry MIMO digital signal processing (DSP) and enabling at the same time MG add/drop at each transit node. Such MGDM system can be employed only in short-reach scenarios, where the differential mode group delays (DMGDs) among the modes belonging to the same mode group can be considered negligible.

On the other hand, MGDM together with partial-MIMO processing has been investigated for increasing the flexibility and the connection provisioning in metro networks [11], [16]; this approach has been analyzed considering the impact on the cumulated IGXT of realistic mode multiplexers (MUX)/demultiplexers (DEMUX) and of propagation in an advanced FMF [17]. Moreover, different node architectures managing the wavelength/spectrum and the mode switching in different ways have been presented and analyzed in terms of required equipment [11], since in a metropolitan scenario one of the main issues is the actual implementation of a network node able to handle both the spectrum and the modes.

In this paper, we extend the work presented in [18], [19], experimentally demonstrating partial-MIMO based MGDM transmission and routing in a cabled 15-mode, 6.1 km FMF, recently deployed in an underground tunnel in the city of L'Aquila, Italy. The 15 spatial modes supported by the employed FMF can be organized in 5 MGs, depending on their respective propagation constants [17]; a full characterization of the deployed FMF cable can be found in [20]. Combined with a multi-plane light conversion (MPLC) [21] based mode MUX/DEMUX, the system had sufficient mode selectivity to support multiple combinations of MGs in MGDM transmission. We evaluate the achievable throughput as a function of the required partial-MIMO receiver resources considering several combinations of MGs as well as various modulation formats [18]. In particular, the performance for 50-Gbaud 4-, 16- and 64- quadrature amplitude modulated (QAM) signals is measured, assuming six co-propagating 75-GHz-spaced WDM channels. Moreover, we show optical add/drop, full-express, and routing operations of three MGs in different multi-hop node scenarios in a 4-node network architecture. We evaluate the impact of the IGXT, introduced by FMF propagation and by the mode MUX/DEMUX employed in each node, on the transmission performance in terms of achievable throughput.

The paper is organized as follows: in Section II, the employed MGDM approach is described, introducing also a suitable system complexity metric useful to compare the performance and the requested DSP resources. In Section III a characterization of the deployed 15-mode FMF-based network is presented, focusing on the MG crosstalk properties of mode MUX/DEMUX and FMF, respectively.

In Section IV the effective number of MIMO taps per equalizer is estimated for different MG configurations, to highlight the impact of uncompensated IGXT on the channel impulse response and the reduction of DSP resources with respect to a full-MIMO approach. The performance of a point-to-point transmission is analyzed for several MG combinations, evaluating the total capacity achievable in function of the employed MIMO resources. The system throughput is estimated applying a suitable error correcting code in case of different modulation formats. It is shown that partial-MIMO MGDM can be used to reduce the required MIMO resources as a function of the desired throughput, allowing to optimize the complexity of the receiver DSP.

In Section V, selected MG configurations are used to demonstrate MGDM routing capabilities in a 4-node network, exploiting several routing scenarios. The reported results demonstrate that MG-based routing is a viable approach to improve flexibility in urban-area networks through space switching at the node level. Finally, conclusions are drawn in Section VI.

II. Mode-Group Division Multiplexing Approach

As previously introduced, in MGDM multiple spatial modes, characterized by similar effective refractive indices, can be organized as a whole super-channel, the MG. In FMFs, the independent MGs are characterized by a weak or even negligible IGXT [10], while the spatial modes belonging to the same MG are strongly coupled, owing to their almost identical propagation constants. The MGDM solution permits to adopt a partial-MIMO approach, in which the processing is applied on a MG basis just on the degenerate modes belonging to the same MG. The complexity of the employed MIMO equalization depends on the number of modes inside the MG, thus permitting to limit the power consumption of the DSP receiver with respect to standard MDM.

An example of MGDM with partial MIMO on 15 spatial modes arranged in 5 MGs is presented in Fig. 1: exploiting a full-MIMO approach, a 30×30 processing should be applied after

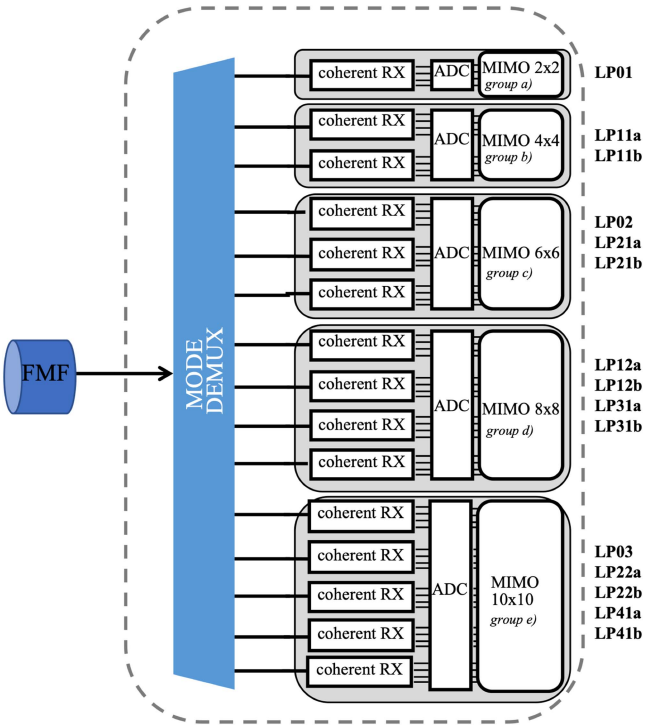

Fig. 1. Example of a MGDM system based on the partial-MIMO approach after coherent detection for a 5 mode-group transmission.

the detection of the 15 modes; thanks to the MGDM solution, instead, each mode group can be processed independently from the others. Furthermore, since the MIMO processing is applied just to compensate the modal coupling inside the specific MG, the MGs can cover different optical paths, allowing the exploitation of the spatial dimension also for routing purposes. On the other hand, the employment of the MIMO equalization only on modes belonging to the same MG leaves a residual uncompensated IGXT after DSP, potentially limiting the performance of the MGDM system in terms of transported capacity and reach.

It is thus important to carefully select combinations of MGs which lead to a limited uncompensated IGXT. For this purpose, both the crosstalk introduced by FMF propagation and mode MUX/DEMUXs needs to be taken into account. Indeed, excluding the MG combinations characterized by excessive IGXT reduces the supported transmission capacity with respect to the full-MIMO approach; however, the improvement in terms of DSP complexity provided by the partial-MIMO approach can be significant. In the following analysis, we quantify this advantage in terms of complexity C, evaluated as the number of required equalizers normalized to a 2×2 MIMO processing, adopted for polarization recovery in standard single mode coherent detection; it is expressed as

$$C = \sum_{i \in \text{ selected MGs}} \frac{2N_i \cdot 2N_i}{2 \cdot 2} = \sum_{i \in \text{ selected MGs}} N_i^2, \quad (1)$$

where N_i refers to the number of spatial modes belonging to mode group i.

Furthermore, the evaluation of the transmission performance is performed by estimating the generalized mutual information

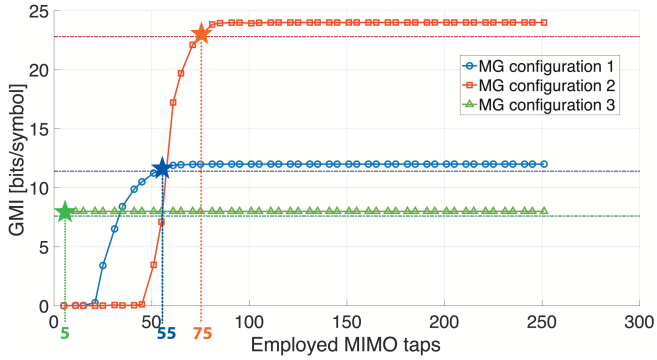

Fig. 2. Examples of effective MIMO taps calculation from the achievable GMI versus the employed number of equalizer taps. Each color represents a different illustrative mode combination. Horizontal dashed-dotted lines: GMI thresholds corresponding to the 95% of the maximum achievable GMI for the specific configuration (Blue: Configuration 1; Red: Configuration 2; Green: Configuration 3). The stars are the selected points on the GMI curve, i.e. they represent the first GMI value greater than the 95% of the achievable GMI for each MG configuration. The corresponding number of taps is reported below (55 taps: Configuration 1; 75 taps: Configuration 2; 5 taps: Configuration 3).

(GMI) as a function of the employed DSP resources, allowing also the assessment of the system throughput achievable by applying a suitable error correcting code [22]. Although the latter may strongly depend on the system implementation, a simple metric based on the effective number of MIMO taps needed at the receiver to correctly recover the transmitted signals has been used. In [18], the effective number of taps was estimated by the complete impulse response composed by 250 taps; here, instead, the effective number is obtained as shown in the example of Fig. 2: the GMI of the specific configuration is evaluated for several lengths of the MIMO equalizers; then, the effective number of taps is selected as the first value that guarantees to reach a GMI greater than the 95% of the maximum GMI achievable by the specific configuration, providing a more rigorous metric. In Fig. 2, the 95% thresholds for the three configurations are shown with dashed-dotted horizontal lines; the selected points are evidenced by the star-symbols, while the corresponding effective number of taps is reported below for each MG configuration.

The analysis on the dependence of the impulse response from the MG, the modulation format and the MG configuration is detailed in Section IV-B, while the performance of multi-MG transmission is evaluated in Section IV-C. As detailed before, to compare the results of different MG combinations, the total number of MIMO taps required by all the MGs employed in the specific configuration is used as metric; this value is calculated as

$$Taps_{tot} = \sum_{i \in \text{ selected MGs}} \tau_i N_i^2, \quad (2)$$

where τ_i represents the effective number of taps per equalizer for MG i in the specific configuration under test.

III. Characterization of the Deployed FMF Testbed

The proposed MGDM system has been experimentally implemented in the SDM testbed deployed in the Italian city of

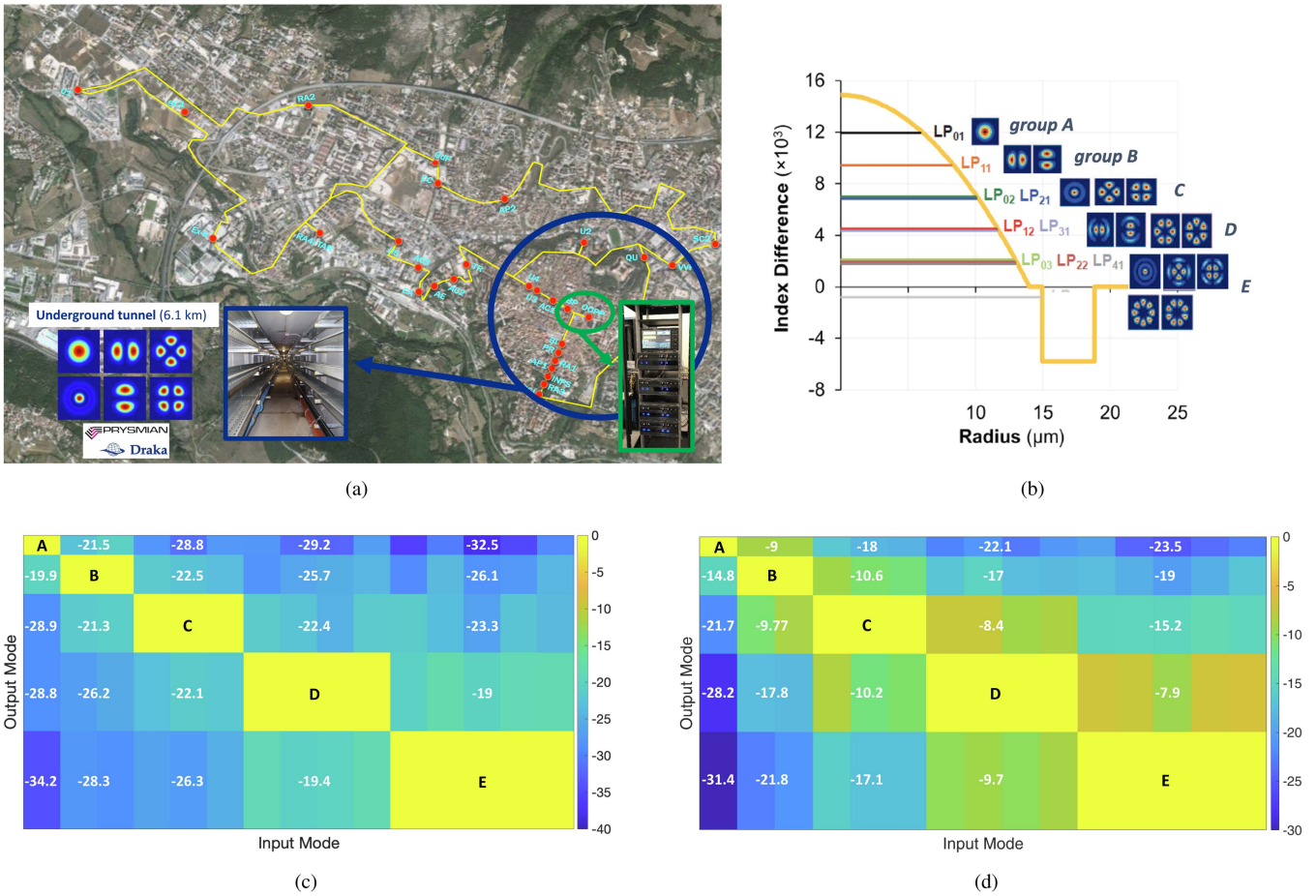

Fig. 3. (a) FMF testbed deployed in L'Aquila city. The red dots on the map denote facilities with access to the larger ring of the metropolitan-area network, which is in the process of being deployed. (b) Intensity distributions and the group classification of the deployed 15-mode FMF. (c) Measured crosstalk matrix of the modal MUX/DEMUX pair. (d) Measured crosstalk matrix at 1556.6 nm wavelength after 6.1km FMF and modal MUX/DEMUX pair.

L'Aquila within project INCIPICT (INnovating CIty Planning through Information and Communications Technology) [23]. The testbed gives access to both coupled and uncoupled multi-core fibers [24], as well as few-mode fibers [20], all deployed in an underground tunnel in a ring configuration (Fig. 3(a)).

The FMF cable used in this work is 6.1-km long and has a conventional structure consisting of six loose tubes surrounding a central strength member, of which two contains four strands of the same 15-mode fiber each. The 15-mode fiber was designed with a trench-assisted, graded-index profile to support 15 spatial modes organized in 5 MGs, depending on their propagation constants. Group A is limited just to the LP01 mode; group B includes LP11a and LP11b; LP02, LP21a and LP21b belong to group C; group D consists of LP12a, LP12b, LP31a, LP31b; group E contains LP03, LP22a, LP22b, LP41a, LP41b. The corresponding intensity distributions and the group classification are shown in Fig. 3(b). Owing to the graded-index profile, a strong coupling is expected among the modes belonging to the same MG; on the other hand, modes belonging to different MGs show a limited crosstalk. Further details on the fiber design and specifications can be found in [17].

To manage the 15 spatial modes supported by the FMF at the transmitter and receiver sides, multi-plane light conversion (MPLC) devices [21], [25] have been used as mode MUX and DEMUX. Their performance in back-to-back conditions have been evaluated in terms of insertion loss and crosstalk, in order to calculate the corresponding values for the 5 MGs. The measured average crosstalk matrix in function of the MG is shown in Fig. 3(c). The reported crosstalk values are averaged on the full C-band, since they are measured exploiting an amplified spontaneous emission (ASE) source at the input port. They are obtained by

$$\mathrm{XT}_{ik} = \frac{\sum_{j \in \mathrm{MG}\, q} P_{ij}}{(\#\mathrm{modes} \in \mathrm{MG}\, q) \cdot \sum_{w \in \mathrm{MG}\, z} P_{iw}} \tag{3}$$

with $mode\ i \in$ MG z and $mode\ k \in$ MG q. The reported equation represents the crosstalk generated by a specific input mode i averaged on all the output modes belonging to mode group q. As a consequence, a single input mode generates the same level of crosstalk on all the modes belonging to another MG, as visible in the reported Figure. Moreover, the crosstalk among modes belonging to the same MG is undefined, since the MGDM approach assumes to treat them as a unique channel. The highest modal crosstalk, generated in back-to-back conditions by the presence of the mode MUX/DEMUX devices, appears in case of adjacent MGs, and it is around -19 dB (between mode group D

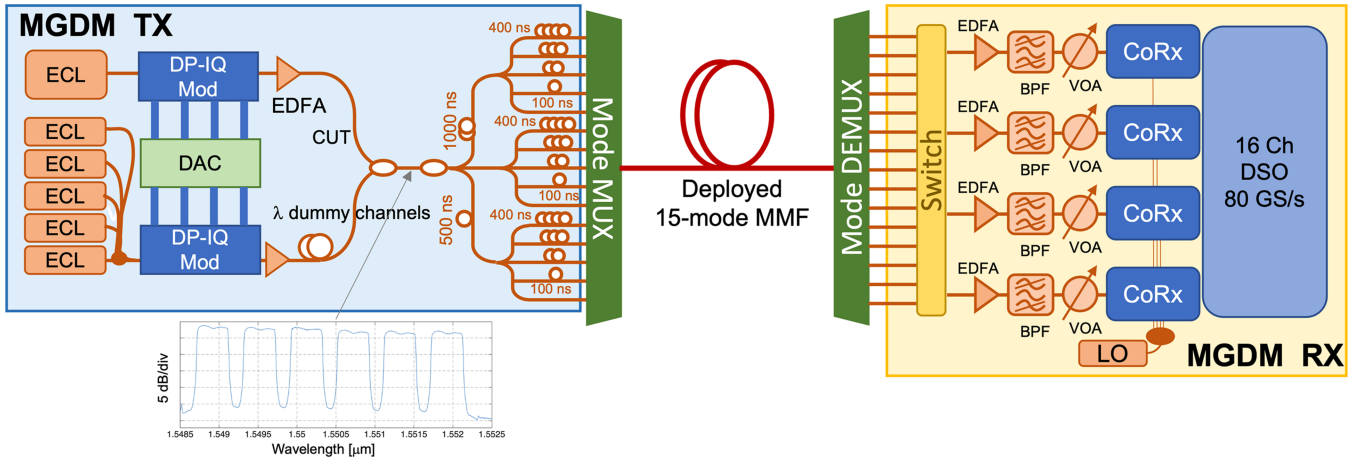

Fig. 4. Point-to-point transmission experimental setup with a deployed MMF cable of 6.1 km

TABLE I
MEASURED AVERAGE INSERTION LOSSES OF THE MPLC MUX DEVICE

MG	A	B	C	D	E
IL [dB]	3.5	3.9	3.87	4.39	4.94

and E); considering distant MGs, on the other hand, the crosstalk is almost negligible, close to −34 dB, as for MGs A and E.

The MPLC device has been characterized also in terms of average insertion losses (ILs) in function of the MG; the measured ILs of a single MPLC MUX/DEMUX device are reported in Table I. The average insertion loss has been calculated as

$$\mathrm{IL}_z = \frac{1}{2}\frac{1}{\#\text{modes} \in \text{MG } z}\sum_{i\in \text{MG } z}\sum_{j\in \text{MG } z}\frac{P_{ij}}{P_{in}} \tag{4}$$

where P_{in} is the optical power at the input port and the factor 2 at the denominator refers to the exploitation of a MUX/DEMUX pair during the measurement. The MG IL is thus calculated taking into account the optical power coupled by a single input mode i to the output ports of all the modes of the specific MG z and then averaging the obtained ILs of all the modes belonging to the same MG. The IL depends on the specific MG, ranging from 3.5 dB of the fundamental mode to about 5 dB for MG E.

Finally, the employed testbed has been characterized in terms of modal crosstalk in presence of the deployed 6.1 km FMF, in order to evaluate its impact on mode mixing during fiber propagation and due to the presence of splices. The measured coupling matrix is shown in Fig. 3(d). A worsening of the XT contribution can be noticed; as before, an undefined coupling among the modes belonging to the same MG is assumed [20]; yet, due to FMF propagation, a stronger coupling among modes of different MGs is present. Nevertheless, distant MGs can be still considered almost independent. In particular, the presence of the 6.1 km FMF generally increases the level of crosstalk, which ranges from -8 dB for adjacent MGs (between MGs C and D and MGs D and E) to −32 dB for distant MGs. Although the measured crosstalks still permit the exploitation of the MGDM approach, a careful selection of the MGs is mandatory, as described in the following Sections. Concerning the different mode loss contributions in the deployed FMF, an attenuation difference < 0.02 dB/km has been estimated [17], leading to a very limited mode-dependent-loss impairment due to FMF propagation.

IV. POINT-TO-POINT IN-FIELD TRANSMISSION

A. Experimental Setup

The experimental setup used to assess the MGDM transmission performance in the field-deployed 15-mode fiber cable is shown in Fig. 4. The light from a tunable external cavity laser (ECL) with a linewidth of less than 100 kHz was modulated by a dual-polarization (DP) IQ-modulator, driven by a 4-channel digital-to-analog converter (DAC). The DAC was operated at 100 GSample/s and it generated a 50 GBaud QAM signal with a cardinality of 4, 16 or 64 with a root-raised cosine shaping with a roll-off factor of 0.01. Five dummy WDM channels were coupled with the channel under test (CUT) with a spacing of 75 GHz (see the inset of Fig. 4); all the 5 signals were modulated by another DP-IQ modulator driven by the negative DAC output ports. The optical carriers of the 6 multiplexed channels ranged from 1549 nm to 1552 nm. The evaluation of the performance has been performed for three CUT configurations, to evidence the insurgence of any wavelength crosstalk/non-linear impairment: in particular, channels 1, 3 and 6 have been measured, characterized by carriers at 1549 nm, 1550.1 nm and 1552 nm, respectively. A split-and-delay method [26] was used to produce 15 optically decorrelated copies of the multiplexed signal with delays of multiples of 100 ns, hence uncorrelated within the length of accumulated differential mode delay in the 15-mode FMF. These signals fed the MPLC mode MUX [21] to be coupled into the deployed graded-index FMF. The 15 spatial modes were transmitted in the following 5 MGs: group A, B, C, D and E, supporting 1, 2, 3, 4 and 5 spatial modes, respectively. As explained in Section II, to limit the insurgence of uncompensated IGXT, only some of the MGs will transport information signals, whereas the remaining will not be illuminated.

After propagation, the spatial channels were demultiplexed by a similar MPLC mode DEMUX and the signals belonging

TABLE II
MODE GROUP COMBINATIONS WITH THE CORRESPONDING NUMBER OF MULTIPLEXED MODES, MIMO COMPLEXITY, AND NUMBER OF EQUALIZERS

Configuration	A	B	C	D	A-B	A-C	A-D	B-D	A-B-D	Full-MIMO
Number of modes	1	2	3	4	3 (1+2)	4 (1+3)	5 (1+4)	6 (2+4)	7 (1+2+4)	15
MIMO complexity	1	4	9	16	5 (1+4)	10 (1+9)	17 (1+16)	20 (4+16)	21 (1+4+16)	225
Number of equalizers	4	16	36	64	20 (4+16)	40 (4+36)	68 (4+64)	80 (16+64)	84 (4+16+64)	900

to a given MG were selected for detection. After amplification in erbium-doped fiber amplifiers (EDFAs) and CUT selection through an optical bandpass filter (BPF), they were sent to up to 4 coherent receivers (CoRxs) and detected using a local oscillator (LO) laser, with a nominal linewidth of less than 100 kHz. The electrical signals from the CoRxs were digitized in 16-channel real-time digital storage oscilloscopes (DSOs) with an electrical bandwidth of 36 GHz, operating at 80 GSample/s. Owing to the availability of just 4 DSOs, MG combinations up to MG D have been experimentally tested. The off-line DSP consisted of a resampling stage to 2 samples per symbol, followed by a time-domain NxN MIMO, with N varying on the number of modes belonging to the specific MG to receive. The MIMO equalizer taps were initially updated using a data-aided least-mean-squares algorithm, which shifted to decision-directed after convergence. Carrier recovery was performed within the equalizer loop, using the algorithm proposed in [27]. After recovering the signal, the DSP estimated the GMI [22], giving the maximum achievable data-rate using a binary soft-decision FEC code, while the bit error rate (BER) was estimated through error counting. The measurements were repeated tuning the CUT wavelength over the spectrum occupied by the WDM grid (inset of Fig. 4).

For the assessment of the performance of the MGDM transmission and routing in the deployed 15-mode FMF cable, we selected 9 suitable MG combinations, considering that we were able to detect simultaneously up to 4 modes, i.e. the complexity corresponding to MG D. Moreover, considering the measured crosstalk (Fig. 3(d)), we excluded the combinations characterized by an excessive IGXT introduced by FMF propagation and mode MUX/DEMUX, since it would drastically impair the performance of the MGDM system. The 9 configurations, their respective number of multiplexed channels and the corresponding complexity of the MIMO processing are reported in Table II [11], [28]; the complexity is calculated following (1). In particular, configurations A, B, C and D are used to assess the reference performance of the specific MG, while combinations A-B, A-C, A-D, B- D and A-B-D are experimented to measure the performance of a MGDM system able to perform MG routing. Due to the limited availability of the DSO equipment, configurations relying on MG E, such as A-E, C-E and A-C-E will be considered in future works. The last configuration reported in Table II refers to the standard full-MIMO approach and it is shown as a benchmark in terms of number of usable modes and DSP complexity needed at the receiver. As expected, the required DSP complexity is lower in case of MGDM with respect to the full-MIMO approach; however, the maximum capacity is limited by the employed number of modes, since the excitation of all the mode groups is not admitted by the presence of uncompensated IGXT. Anyway, the 3-MG configuration taken into account shows a required complexity one order of magnitude lower than the full-MIMO one.

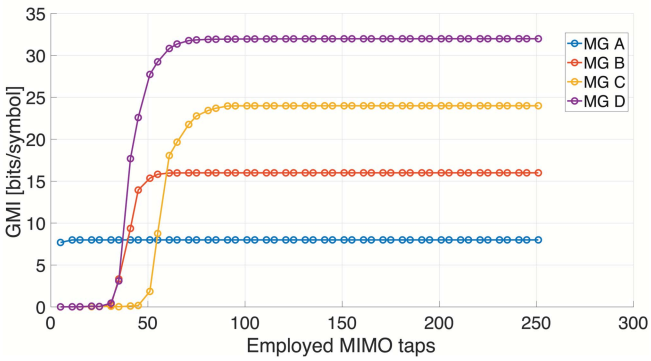

Fig. 5. GMI convergence in function of the employed MIMO taps per equalizer for mode group A (blue), B (red), C (orange) and D (purple). The curves are obtained in case of a single MG propagating in the deployed FMF with 16-QAM modulation format.

The evaluation of their transmission performance allowed the estimation of the system throughput, as a function of the employed DSP resources, obtained from the effective MIMO taps number per equalizer measured for each configuration, as explained in Section II.

B. *Effective MIMO Taps Analysis*

At first, the response of the fiber channel has been measured. In particular, its effective time duration has been measured, evaluating the number of MIMO taps needed to correctly recover the transmitted signal. The effective number of taps has been calculated observing the convergence of the GMI with respect to the employed number of MIMO taps; the analysis has been performed varying the specific MG under test, the modulation format and the MGDM configuration. The results are shown in Figs. 5–7, respectively. As explained in Section II, the effective number of taps is calculated by selecting the value that guarantees a GMI of 95% of the maximum achievable GMI for the specific configuration. The MIMO taps used in the processing are varied in the range $5-250$, corresponding to an impulse response time duration ranging from 62.5 ps to 3.125 ns, respectively. When different MGs are simultaneously transmitted, the effective number of MIMO taps has been estimated separately for each MG.

Examples of GMI convergence for MG A, B, C and D at a wavelength of 1550.1 nm are shown in Fig. 5. The reported curves are obtained in case of a single MG propagating in the deployed FMF with the same modulation format (16-QAM). The convergence time increases with the number of spatial modes belonging to the specific MG: MG A, composed by just a single

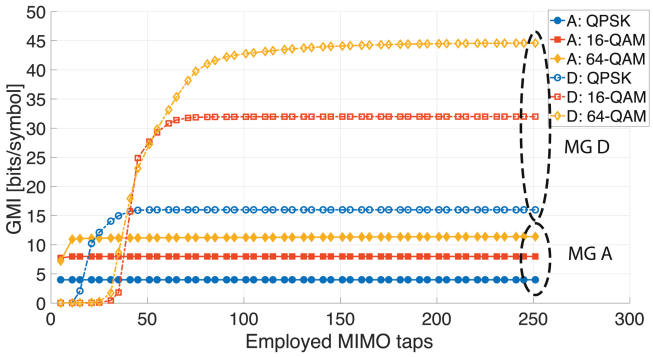

Fig. 6. GMI in function of the employed MIMO taps per equalizer for mode groups A (continuous lines, full marks) and D (dashed-dotted lines, open marks) for different modulation formats (QPSK: Blue; 16-QAM: Red; 64-QAM: Orange).

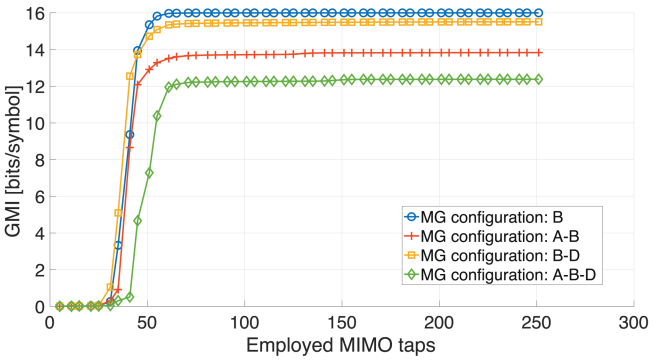

(a) Mode group B.

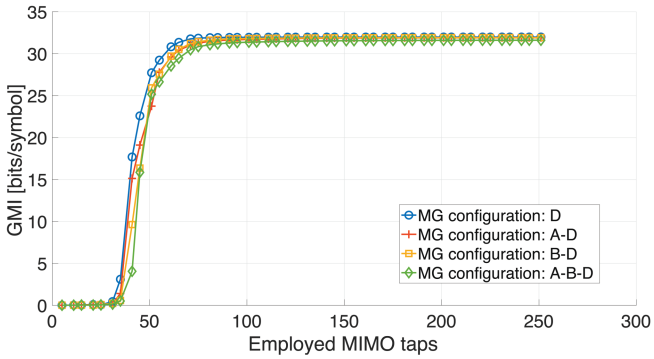

(b) Mode group D.

Fig. 7. GMI versus the employed number of MIMO taps per equalizer for (a) mode group B and (b) mode group D for different MGDM configurations. The reported number of taps is related to the recovery of the modes belonging to the proper MG under test in the specific MG configuration detailed in the legend.

spatial mode, shows a quick convergence to the maximum value, while MG B, C and D are characterized by a larger convergence time. This increase is caused by the spread of the spatial modes belonging to the specific MG during fiber propagation. However, the increase is not proportional to the number of spatial modes: both MG B and MG D start to converge after 35 taps, while MG C from 51 taps.

Fig. 6 shows the GMI convergence calculated for MG A and D at a wavelength of 1550.1 nm in case of different modulation formats (QPSK, 16-QAM and 64-QAM) when only the selected MG is propagating in the deployed FMF network. In [18], owing to the effective taps number estimation by the complete impulse response, a negligible dependence on the modulation format was obtained. Here, instead, the new metric obtained by an actual number of MIMO taps results in a difference between the modulation formats, as lower-order formats can be optimally recovered even by a minimal number of MIMO taps. In case of MG A, the modulation format has a negligible impact on the GMI convergence, since the maximum achievable value is reached with few MIMO taps. On the other hand, when MG D is employed, the GMI convergence depends on the modulation format, requiring more MIMO taps in case of higher-order QAM.

TABLE III
AVERAGE EFFECTIVE NUMBER OF TAPS PER EQUALIZER FOR THE ANALYZED MODE GROUP CONFIGURATIONS

MG	QPSK	16-QAM	64-QAM
A	5	5	12
B	35	50	64
C	54	80	92
D	41	65	98
A-B	5; 38	11; 58	-
A-C	5; 54	8; 78	11; 92
A-D	5; 46	5; 70	11; 102
B-D	37; 42	55; 67	64; 96
A-B-D	6; 42; 42	15; 62; 73	-

Finally, a comparison of the GMI convergence for different MGDM configurations is reported in Fig. 7 both for MG B and MG D. The presence of several MGs co-propagating in the same 6.1-km deployed FMF has a negligible impact for MG D, as highlighted by the superposition of the convergence curves reported in Fig. 7(b). No difference among the measured GMIs can be noticed, since in the employed configurations MG D is never propagating with an adjacent MG. On the other hand, when the transmission system employs adjacent MGs, as shown in Fig. 7(a) for A-B and A-B-D configurations, an increase of the MIMO taps needed to recover the signals appears; moreover, a reduction in the achievable GMI can be noticed, owing to the residual IGXT that cannot be cancelled by the employed technique.

The GMI convergence curves have been used to calculate the average effective number of taps needed to correctly recover the transmitted signals by the MG-based MIMO equalizers for each specific MG combination. The results are reported in Table III for the three possible modulation formats and for all the employed MGs present in the different configurations.

As expected, the average number of taps increases with the MG order, even though the effective number doesn't follow a linear trend. Only when adjacent MGs are employed, the presence of other co-propagating MGs causes a slight increase in the number of MIMO taps needed with respect to the single MG configuration. This increase is more evident in case of higher-order modulation formats when more MGs are propagating, as in case of 16-QAM in the A-B-D configuration. When adjacent MGs are used, 64-QAM cannot be properly recovered, thus no indication in terms of MIMO taps is reported.

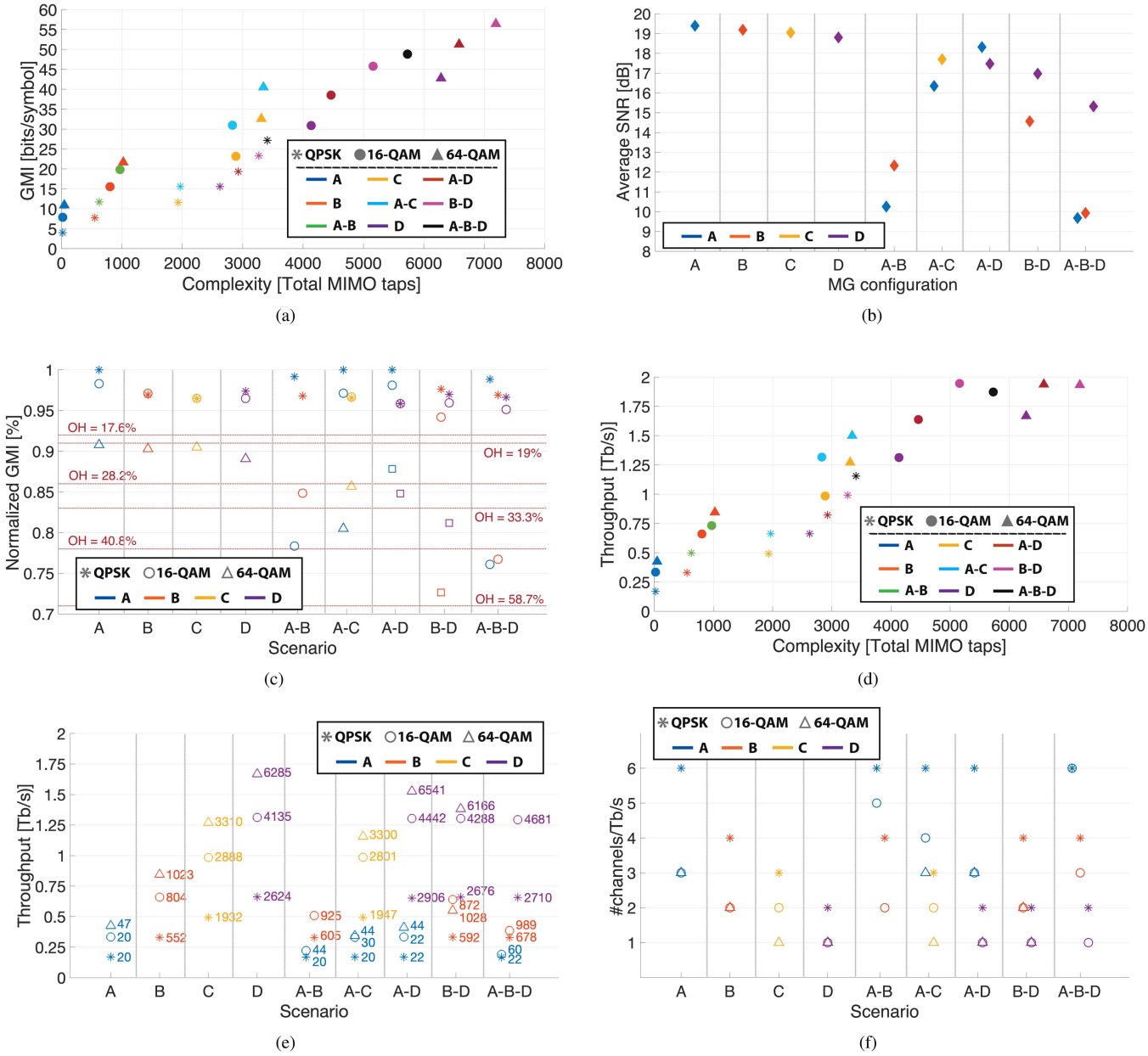

Fig. 8. (a) Experimental results of partial-MIMO MGDM transmission per MG combination versus resources in terms of total MIMO taps: GMI per 50-Gbaud wavelength channel. (b) Achievable SNRs in the different mode-group configurations. (c) Calculated NGMI for the different MG configurations with thresholds of the employed error correcting codes and corresponding OHs (red dotted lines). (d) Experimental results of partial-MIMO MDM transmission per MG combination versus resources in terms of total MIMO taps: decoded throughput for a single 50-Gbaud WDM channel. (e) Achieved net-throughput for the three employed modulation formats for each MG configuration; the requested total number of taps for the specific mode/channel is reported on the right side of each point. (f) Minimum number of WDM channels needed to transmit 1 Tb/s using the different MGs for the three modulation formats. The different modulation formats are represented in the reported figures by asterisks (QPSK), circles (16-QAM), and triangles (64-QAM).

The calculated effective number of taps needed for each MG configuration has been used to define a simple metric of the complexity of the proposed solution, evaluated in terms of necessary DSP resources in the different propagation conditions. The corresponding measured performance are shown in the next Section.

C. Transmission Results

Fig. 8(a) shows the GMI per wavelength channel per MG combination for 50 Gbaud QPSK (asterisks), 16-QAM (circles) and 64-QAM (triangles) signals, with the colors representing different MG combinations. As expected, the GMI increases with the number of utilized MGs at the expense of a higher MIMO complexity, calculated following (2). On the other hand, the use of a partial-MIMO strategy permits to exploit different MGs for advanced mode routing, simultaneously limiting the required equalizer MIMO taps with respect to the full-MIMO solution, although at the expense of IGXT impairments on the performance. If we consider a 7-mode transmission, as in case of A-B-D combination, the full 30×30 MIMO complexity would have been more than one order of magnitude higher [20] than

the MGDM approach of this work, composed by the sum of a 2 × 2, a 4 × 4 and a 8 × 8 MIMO processing. Moreover, sometimes the same transported capacity can be achieved using different MG configurations, thus it is possible to choose the optimal MG combination that permits to limit the needed MIMO complexity. A clear example is the configuration A-C that allows to obtain the same GMI of MG D for both QPSK and 16-QAM modulation formats, but with a reduced MIMO complexity; the performance of 64-QAM is instead limited by the residual IGXT between the two mode groups. The strongest impact of IGXT on the GMI performance appears on group configurations A-B and A-B-D, where the quality of 64-QAM modulated signals is severely degraded due to the strong crosstalk between groups A and B, preventing the exploitation of such a modulation format.

The signal-to-noise ratios (SNRs) achievable in the different mode-group configurations is reported in Fig. 8(b). The SNR is estimated by the bit error rate (BER) measured for each mode group. The 4 single configurations (A, B, C, D) show similar SNR values, since no residual IGXT is present. In these conditions, the SNR is close to 19 dB, corresponding to the system reference SNR, with a slight decrease for higher-order MGs. For the other 5 configurations, lower SNR values are achieved, and sometimes strong differences between the MGs can be noticed. The lowering of the SNR is due to the presence of uncompensated IGXT, which assumes different levels for different co-propagating MGs. Two configurations appear strongly impaired: in case of A-B and A-B-D configurations, mode groups A and B show SNRs close to 10–12 dB. For configuration A-B, the most impaired MG is the first one, since the optical power sent on MG B is two times the MG A one. In configuration A-B-D, mode group D still shows good SNR performance, thanks to its distance from the other co-propagating MGs. The SNR of MG B is anyhow reduced with respect to the previous configuration, owing to the additional presence of MG D, which slightly affects even MG A. The evidenced impairments influence the achievable GMI already reported in Fig. 8(a) and, especially, the throughput performance shown in Fig. 8(d). If a single MG configuration is used (A, B, C and D configurations), the GMI increase is proportional to the number of the transmitted spatial modes, thanks to the MIMO processing that correctly recovers all the transmitted signals. On the other hand, when multi-MG configurations are considered, the presence of the residual IGXT cannot be compensated by the MIMO processing, leading to a degradation of the system performance. The penalty appears as a reduction of the GMI with respect to the maximum achievable one, which can be calculated as the sum of all the GMIs related to the employed MGs in a single-MG configuration. The impact of the simultaneous presence of several MGs on the GMI performance is more severe for MG combinations including adjacent MGs (A-B and A-B-D configurations).

The GMI values shown in Fig. 8(a) permit to calculate the net throughput achievable for the specific MG configuration by applying bit-wise decoding and optimal variable-rate codes, obtained by the concatenation of suitable soft-decision (low-density parity check - LDPC or Turbo) error correction and of a Staircase code [22]. To obtain an accurate prediction of the post-FEC performance, normalized GMI (NGMI) is assumed as the best metric to be used. Fig. 8(c) shows the NGMI corresponding to the different MGs for the several exploited configurations, evidencing also the performance varying the modulation format. Moreover, the thresholds corresponding to the different error correcting codes with their overall overhead (OH) are reported. For all the MG configurations taken into account, the NGMI is higher than 95% in case of QPSK modulation, thanks to its resilience to optical noise and limited SNR. In the 4 single MG configurations (A, B, C, D), 16-QAM performs similarly to QPSK, while 64-QAM shows a reduction, owing both to the 95% threshold on the maximum achievable GMI applied for the evaluation of the effective MIMO taps and to the SNR that is not enough to maintain a negligible BER; in this case, the NGMI doesn't permit to apply the most efficient decoding, since its values fall in the second or even third code working regions. In the other MG configurations, 16-QAM and 64-QAM perform worse, as expected by the SNR analysis presented before. In particular, the uncompensated IGXT impacts only 64-QAM performance for configurations A-C, A-D and B-D, thanks to the distance between the co-propagating MGs; for A-B and A-B-D configuration, instead, even 16-QAM performance is strongly reduced, owing to the IGXT cumulated by adjacent mode groups. Comparing the performance of 16-QAM for A-B and C configurations (3 propagating modes) and of 64-QAM for A-C and D configurations (4 propagating modes), a clear reduction of the performance is present in case of multiple-MG exploitation. In these conditions, even though the number of modes employed in the transmission is the same, the exploitation of different MGs leads to the presence of uncompensated IGXT that can limit the performance of the system. Thus, for the two considered cases, the total MIMO complexity reduction is paid at the expense of a penalty on the system capacity.

Fig. 8(d) shows the achieved net-throughput per wavelength estimated from the GMI after the decoding with a binary soft-decision FEC code and a receiver applying bit-wise decoding and optimal variable-rate codes [22]. As can be seen, almost 2 Tb/s throughput can be obtained using 50 Gbaud 64-QAM modulation both with A-D and B-D MG configurations. Interestingly, the same throughput per channel can be achieved with a lower MIMO complexity using B-D configuration with 16-QAM modulation, not showing any advantage in the exploitation of 64-QAM in case of multi-MG transmission. Observing Fig. 8(a), a difference of about 10 bits/symbol is present between the two modulation formats for B-D configuration; however, since the NGMI is strongly limited in presence of 64-QAM format, no net-throughput increase appears. With respect to Fig. 8(a), B-D 64-QAM decoded throughput is close to the A-D one, since a lower rate FEC is necessary owing to the lower SNR value of this configuration; this effect is confirmed by the corresponding NGMI, reducing the advantage of having a larger number of transmitted modes. For the same reason, the 3-tuple A-B-D is impaired by IGXT between groups A and B, strongly limiting the performance even of 16-QAM modulation, which is lower than the achieved one in case of B-D configuration, which is characterized by a lower number of modes and complexity;

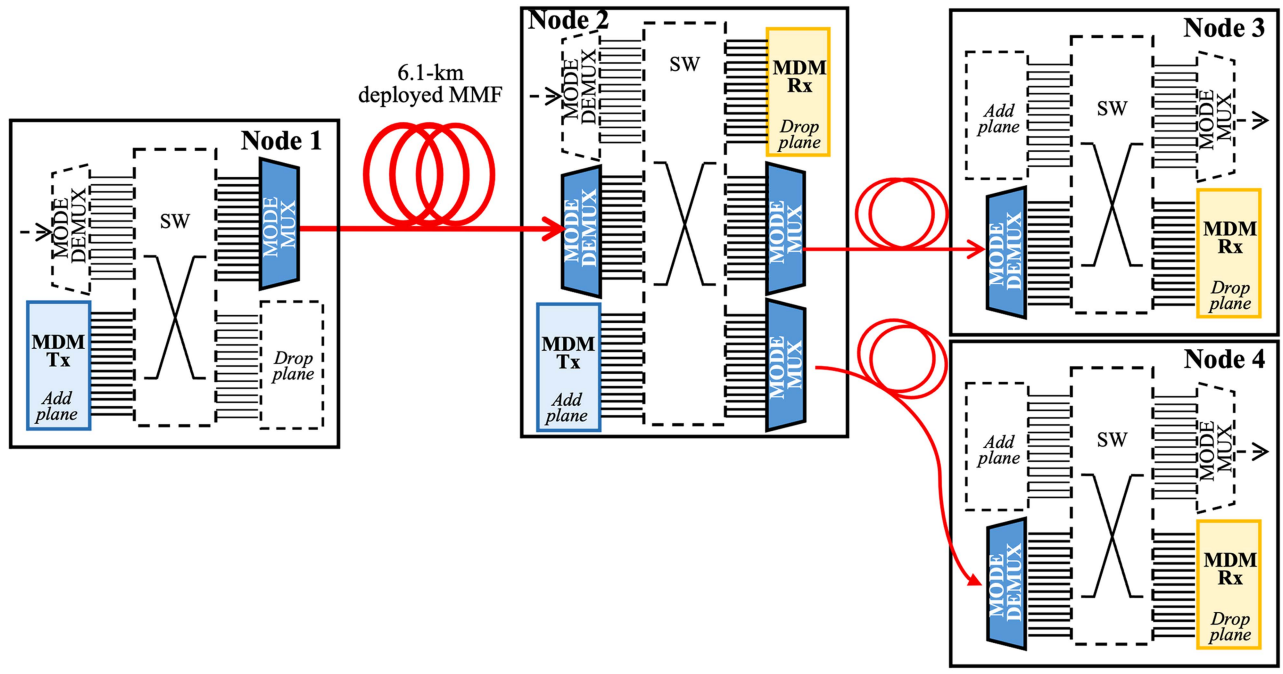

(a)

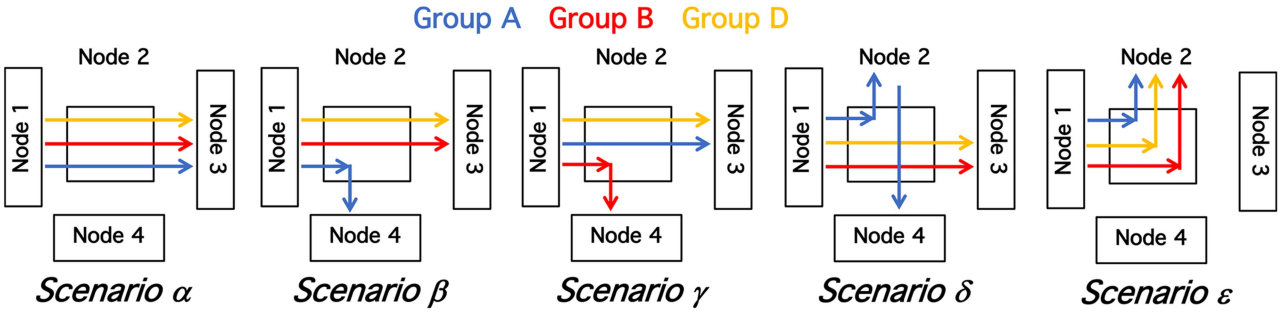

(b)

Fig. 9. (a) Experimental setup for MG-based multi-hop routing. Light blue and yellow boxes are the MGDM Tx and MGDM Rx described in Section IV. (b) Multi-hop routing scenarios experimented in the testbed considering four nodes.

anyway, in the A-B-D case all the 3 MGs could be used for MG routing [11]. Exploiting the full C-band and considering the per-channel performance demonstrated, a cumulative data-rate $\approx$ 80 Tb/s can be achieved, using a limited complexity MIMO DSP with approximately 5000 taps per WDM channel.

Fig. 8(e) details the achieved net-throughput in the different MG configurations for the three employed modulation formats; the requested total number of taps for the specific mode/channel is reported on the right side of each point. Considering the four reference scenarios, a linear increase of the transported capacity with respect to the number of modes belonging to the MG can be noticed. Moreover, a significant reduction in the throughput for 64-QAM appears, as expected by the previous analysis: it is not possible to reach a factor 3 between QPSK and 64-QAM as theoretically expected, but at most a factor 2.5 is obtained. This limit in the capacity for higher-order modulation formats is due to both the channel SNR, which is not enough to sustain the 64-QAM format, and to the selected 95% threshold applied for effective MIMO taps calculation. In the multi-MG configurations, on the other hand, a strong reduction in the net throughput appears in case of adjacent MGs for modulation formats beyond 16-QAM, impacting all the exploited MGs. In particular, comparing A-B, B-D and A-B-D configurations, a negligible variation is present on the MG D performance, thanks to the absence of its adjacent MGs. On the other hand, MG B is strongly affected by the presence of MG A; moreover, the co-propagation of MG D, in the A-B-D configuration, although not adjacent to MG B, is sufficient to introduce an additional uncompensated IGXT reducing the throughput for 16-QAM. The same effect is shown by B-D configuration, for which the 64-QAM capacity is reduced with respect to the 16-QAM one in case of MG B. Similarly, 64-QAM throughput is reduced in case of A-C configuration. Finally, when the employed MGs are quite distant, as in the case of A-D configuration, just a slight reduction can be noticed for 64-QAM for the most complex MG (i.e. MG D). As already reported, the total number of MIMO taps doesn't show a strong variation in function of the scenario, with a marginal increase in case of adjacent MG presence.

As expected, in case of higher-order MGs both the total number of taps and the net throughput increase, improving the spectral efficiency. It is thus interesting to evaluate the impact of the MG choice on the number of employed spectral resources (i.e. WDM channels). Fig. 8(f) shows the minimum number of WDM channels needed to transmit 1 Tb/s using the different MGs for the three modulation formats. This target capacity can be achieved using just one WDM channel in case of MG D with 16- or 64-QAM and of MG C with 64-QAM, while the other MGs/configurations require at least 2 WDM channels and higher modulation formats. The maximum number of channels is required by the lowest-complexity solution, i.e. QPSK on MG A that needs up to 6 WDM channels. Spectral resource saving is thus paid at the expense of higher DSP complexity.

V. Mode-Group Division Multiplexing for Routing

MGDM is a potential solution to improve the granularity in switching and to enable a multi-hop routing scenario. Thanks to MGDM, modes belonging to the same MG can be aggregated/dropped in an all-optical way and handled at the node level, operating simultaneously in both spectrum and space dimensions [11]. In this Section, the in-field demonstration of MG routing is reported for different network architectures [19].

A. In-Field Network Demonstration Scenario

Fig. 9(a) shows the setup used to evaluate an optical network composed by 4 nodes. The nodes provide mode handling and add&drop modules, as described in [11]. The MGDM transmitter (Tx) and receiver (Rx) blocks, labeled by light blue and yellow boxes in Fig. 9(a), have been previously presented in Fig. 4. As described in Section IV-A, the six 50-Gbaud DP M-QAM 75-GHz spaced WDM channels are transmitted in the 15 spatial modes supported by the FMF using a split-and-delay setup. At the MGDM receiver, after WDM channel selection, coherent detection and demodulation and partial MIMO equalization are performed for the modes within the same MG. In each node, a pair of 15-mode MPLC mode MUX/DEMUX [21] was employed. The dashed blocks in Fig. 9(a) were not implemented in the experimental setup: in particular, the spatial switch (SW) operation in each node was performed manually. From the preliminary characterization of the deployed network reported in Section IV-A, the uncompensated IGXT is not negligible between neighbor MGs, arising at most from the mode MUX/DEMUX. IGXT thus represented the main limitation for MG-based multi-hop routing, particularly considering that the IGXT introduced by the FMF propagation is small for metro links of a few kilometres.

Section IV-A results allowed us to select, for the MG routing demonstration, the combination of excited MGs involving group A, group B and group D. Fig. 9(b) reports the routing scenarios tested in the experimentation in the A-B-D configuration. In particular, node 2 enables also the selection of the proper output direction, with nodal degree 3. Scenario α implements full-express operation; scenario ϵ is the full-drop of the three MGs; scenario δ corresponds to the partial add/drop for the group A; finally, scenario β and γ represent the routing in different directions. All the three MGs co-propagate in the fiber link connecting node 1 and 2, corresponding to the 6.1 km deployed FMF, allowing the evaluation of the impact of the IGXT introduced by propagation over typical metro-haul distances. The connection between node 2 and 3 and node 2 and 4 is, on the other hand, short (less than 100 m) in order to mainly estimate the impact of the mode MUX/DEMUX operating in each node.

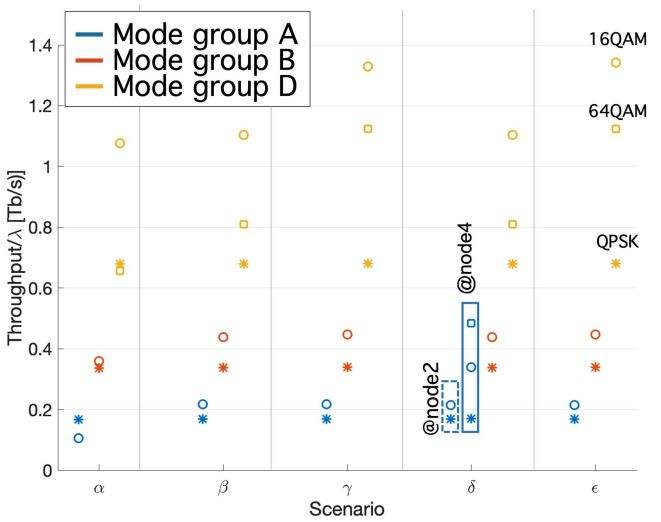

Fig. 10. Decoded measured throughput for the different scenarios per MG and per wavelength. Modulation formats: QPSK (asterisks); 16-QAM (circles); 64-QAM (squares).

B. MG Routing Results

Fig. 10 shows the throughput achievable for each group per single wavelength (for the three M-QAM modulations) in the considered routing scenarios (Fig. 9(b)). In particular, in scenario ϵ, corresponding to the full-drop of all the three MGs, the group A and B coming from node 1 are limited by the mutual IGXT, affecting above all the higher-order QAM formats. Their performance in terms of achievable rate per group is further limited in scenario α (three groups full-express), owing to the additional mode MUX/DEMUX pair required for the second hop. In scenario δ, the additional group A added at node 2 and routed to node 4 is not limited by IGXT. Moreover, the group A coming from node 1 and dropped at node 2 (1 hop) has similar performance to the scenario β, where group A performs 2 hops, but without the IGXT added in the second mode MUX/DEMUX. In scenario γ, group D throughput is negligibly affected by the IGXT introduced by the presence of A in the second node MUX/DEMUX. Its performance decreases in scenario β and δ, when group D is limited by the presence of group B at the second node MUX/DEMUX.

In Table IV, we report the maximum decoded throughput measured per each MG in the experimented routing scenarios: considering all the 6 WDM 75-GHz spaced channels, Tb/s routing capabilities can be achieved. As previously demonstrated in Section IV, the maximum capacity seldom corresponds to the 64-QAM modulation, which is less robust to the IGXT

TABLE IV
WDM MAXIMUM DECODED THROUGHPUT PER MG [TB/S]

Routing scenario	Group A	Group B	Group D
α	@node3: 1	@node3: 2.16	@node3: 6.46
β	@node4: 1.3	@node3: 2.63	@node3: 6.62
γ	@node3: 1.3	@node4: 2.7	@node3: 7.98
δ	@node2: 1.28 @node4: 2.91	@node3: 2.16	@node3: 6.46
ϵ	@node2: 1.28	@node2: 2.68	@node2: 8.05

impairment, requiring lower-rate error correcting codes and, thus, actually reducing the net transported capacity.

VI. CONCLUSION

We demonstrated the capabilities of MGDM for space multiplexing and routing in the first deployed 15-mode FMF network in the city of L'Aquila, Italy. Thanks to MGDM, a significant reduction of the requested DSP resources is achieved, exploiting a partial-MIMO approach that operates separately on the different MGs. This processing permits to handle the polarization diversity and the mode degeneracy for the modes belonging to the same MG, but significantly simplifying the receiver configuration and strongly reducing the number of resources in terms of taps for MIMO equalization with respect to the classical full-MIMO approach. The presence of residual uncompensated IGXT introduced by FMF propagation, over distances typical of urban applications, and by the mode MUX/DEMUX has been analyzed.

Several MG combinations and QAM modulation formats have been considered, in order to measure the impact of the uncompensated IGXT at the receiver end in different system configurations. The performance of the proposed solution has been analyzed in terms of total capacity achievable in the different MG scenarios, exploiting as a suitable metric of the complexity of the employed system the effective number of MIMO taps, i.e. the taps needed to reach the 95% of the maximum achievable performance. The performed analysis has shown that the effective number of taps is normally in the range of $20 - 70$ taps per MIMO equalizer, with a slight increase in case of higher-order MGs, multi-MG configurations and modulation formats. The calculated requested resources reduce of more than a factor 10 the complexity of the system with respect to a standard full-MIMO approach. The performance of a 6.1 km-long point-to-point connection has been measured, obtaining that a total net throughput of almost 2 Tb/s per WDM channel can be achieved, exploiting a multi-MG solution with 2 or 3 MGs simultaneously propagating in the same FMF. Considering the full C-band, a total net throughput of $\approx$80 Tb/s can be transmitted on a single 15-mode FMF link. In FMF supporting more propagating modes, a careful selection of MGs would permit to even increase the performance of the partial-MIMO solution, given that non-adjacent MGs are used to limit the insurgence of uncompensated crosstalk.

Then, we experimentally demonstrated the capabilities of space switching based on the routing of groups of degenerate spatial modes in urban networks, useful for improving the network flexibility at the node level. The feasibility of MG-based routing has been tested in the deployed 5-group FMF ring network, considering a network architecture composed by 4 nodes with mode-handling capabilities. Several routing scenarios have been tested, ranging from full-express/full-drop to partial add/drop operations, to highlight the effect of FMF propagation and MUX/DEMUX presence on the system performance. The results have shown that IGXT impairment, affecting the maximum allowed throughput, seems to arise both within the mode MUX/DEMUX and the short FMF transmission spans in the urban scenario. As discussed in [11], MGDM is suitable for short- and medium- reach networks, where residual uncompensated IGXT is limited. Network scalability can be pursued improving MUX/ DEMUX performance and using FMFs allowing the selection of suitable combinations of MGs showing minimal residual uncompensated IGXT. In the experimented 3 MG system, Tb/s routing has been demonstrated, showing that MGDM is an interesting solution to increase both the transmission throughput and the network flexibility exploiting limited DSP resources.

REFERENCES

[1] K.-i. Kitayama and N.-P. Diamantopoulos, "Few-mode optical fibers: Original motivation and recent progress," *IEEE Commun. Mag.*, vol. 55, no. 8, pp. 163–169, Aug. 2017.

[2] R. Ryf et al., "Mode-division multiplexing over 96 km of few-mode fiber using coherent 6 × 6 MIMO processing," *J. Lightw. Technol.*, vol. 30, no. 4, pp. 521–531, Feb. 2012.

[3] L. Dallachiesa et al., "Mode-group-division multiplexing over a deployed 15-mode-fiber cable," in *Proc. IEEE Opt. Fiber Commun. Conf. Exhib.*, 2023, pp. 1–3. [Online]. Available: https://opg.optica.org/abstract.cfm?URI=OFC-2023-M2B.4

[4] R. S. Luis et al., "Dynamic crosstalk and skew on a 1.3 TB/S full-duplex O-band short reach transmission using an 8-core fiber," in *Proc. 45th Eur. Conf. Opt. Commun.*, 2019, pp. 1–4.

[5] R. Munoz et al., "Adaptive software defined networking control of space division multiplexing super-channels exploiting the spatial-mode dimension," *J. Opt. Commun. Netw.*, vol. 12, no. 1, pp. A58–A69, Jan. 2020.

[6] F. Arpanaei, N. Ardalani, H. Beyranvand, and S. A. Alavian, "Three-dimensional resource allocation in space division multiplexing elastic optical networks," *J. Opt. Commun. Netw.*, vol. 10, no. 12, pp. 959–974, Dec. 2018.

[7] D. Soma, Y. Wakayama, K. Igarashi, and T. Tsuritani, "Partial MIMO-based 10-mode-multiplexed transmission over 81km weakly-coupled few-mode fiber," in *Proc. Opt. Fiber Commun. Conf. Exhib.*, 2017, pp. 1–3.

[8] S. Sumita, D. Soma, S. Beppu, Y. Wakayama, H. Takahashi, and T. Tsuritani, "Experimental evaluation on switching operation for mode and wavelength switched network (M-WSON) using weakly-coupled few-mode fiber," in *Proc. 23rd Opto- Electron. Commun. Conf.*, 2018, pp. 1–2.

[9] C. E. M. Rottondi, P. Martelli, P. Boffi, and M. Tornatore, "Transceivers and spectrum usage minimization in few-mode optical networks," *J. Lightw. Technol.*, vol. 37, no. 16, pp. 4030–4040, Aug. 2019.

[10] R. Rumipamba-Zambrano, R. Muñoz, R. Casellas, J. Perelló, S. Spadaro, and A. E. Elfiqi, "Design and assessment of FM-MCFs-suited SDM-ROADMs with versatile spatial group configurations and unified QoT estimator," *J. Lightw. Technol.*, vol. 38, no. 22, pp. 6137–6152, Nov. 2020.

[11] P. Boffi et al., "Mode-group division multiplexing: Transmission, node architecture, and provisioning," *J. Lightw. Technol.*, vol. 40, no. 8, pp. 2378–2389, Apr. 2022.

[12] C. Rottondi, P. Boffi, P. Martelli, and M. Tornatore, "Routing, modulation format, baud rate and spectrum allocation in optical metro rings with flexible grid and few-mode transmission," *J. Lightw. Technol.*, vol. 35, no. 1, pp. 61–70, Jan. 2017.

[13] K. Benyahya et al., "Multiterabit transmission over OM2 multimode fiber with wavelength and mode group multiplexing and direct detection," *J. Lightw. Technol.*, vol. 36, no. 2, pp. 355–360, Jan. 2018.

[14] J. Li et al., "Terabit mode division multiplexing discrete multitone signal transmission over OM2 multimode fiber," *IEEE J. Sel. Topics Quantum Electron.*, vol. 26, no. 4, Jul./Aug. 2020, Art. no. 4501308.

[15] A. Gatto, P. Martelli, P. Parolari, N. Sambo, P. Castoldi, and P. Boffi, "Mode group division multiplexing in 5 mode-group FMF enabling MIMO-free solutions," *IEEE Photon. Technol. Lett.*, vol. 34, no. 21, pp. 1167–1170, Nov. 2022.

[16] N. Sambo, P. Martelli, P. Parolari, A. Gatto, P. Castoldi, and P. Boffi, "Mode-group division multiplexing for provisioning in SDM networks," in *Proc. Eur. Conf. Opt. Commun.*, 2020, pp. 1–4.

[17] P. Sillard et al., "Low-differential-mode-group-delay 9-LP-mode fiber," *J. Lightw. Technol.*, vol. 34, no. 2, pp. 425–430, Jan. 2016.

[18] A. Gatto et al., "Partial MIMO-based mode division multiplexing transmission over the first field-deployed 15-mode fiber in metro scenario," in *Proc. IEEE Opt. Fiber Commun. Conf. Exhib.*, 2023, pp. 1–3. [Online]. Available: https://opg.optica.org/abstract.cfm?URI=OFC-2023-M2B.3

[19] P. Parolari et al., "Demonstration of multi-hop mode-group routing in a field-deployed multi-mode fiber network," in *Proc. IEEE Opt. Fiber Commun. Conf. Exhib.*, 2023, pp. 1–3. [Online]. Available: https://opg.optica.org/abstract.cfm?URI=OFC-2023-M4G.3

[20] G. Rademacher et al., "Characterization of the first field-deployed 15-mode fiber cable for high density space-division multiplexing," in *Proc. Eur. Conf. Opt. Commun.*, 2022, pp. 1–4.

[21] N. Barre, B. Denolle, P. Jian, J.-F. Morizur, and G. Labroille, "Broadband, mode-selective 15-mode multiplexer based on multi-plane light conversion," in *Proc. Opt. Fiber Commun. Conf. Exhib.*, 2017, pp. 1–3.

[22] A. Alvarado, E. Agrell, D. Lavery, R. Maher, and P. Bayvel, "Replacing the soft-decision FEC limit paradigm in the design of optical communication systems," *J. Lightw. Technol.*, vol. 34, no. 2, pp. 4338-4352, Oct. 2015.

[23] C. Antonelli et al., "The city of L'Aquila as a living lab: The INCIPICT project and the 5G trial," in *Proc. IEEE 5G World Forum*, 2018, pp. 410–415.

[24] T. Hayashi et al., "Field-deployed multi-core fiber testbed," in *Proc. 24th OptoElectronics Commun. Conf. Int. Conf. Photon. Switching Comput.*, 2019, pp. 1–3.

[25] G. Labroille, B. Denolle, P. Jian, P. Genevaux, N. Treps, and J.-F. Morizur, "Efficient and mode selective spatial mode multiplexer based on multi-plane light conversion," *Opt. Exp.*, vol. 22, no. 13, pp. 15599–15607, Jun. 2014. [Online]. Available: https://opg.optica.org/oe/abstract.cfm?URI=oe-22-13-15599

[26] G. Rademacher et al., "Peta-bit-per-second optical communications system using a standard cladding diameter 15-mode fiber," *Nature Commun.*, vol. 12, 2021, Art. no. 4238.

[27] T. Pfau, S. Hoffmann, and R. Noe, "Hardware-efficient coherent digital receiver concept with feedforward carrier recovery for M -QAM constellations," *J. Lightw. Technol.*, vol. 27, no. 8, pp. 989–999, Apr. 2009.

[28] S. Randel et al., "6 $\times$ 56-Gb/s mode-division multiplexed transmission over 33-km few-mode fiber enabled by 6 $\times$ 6 MIMO equalization," *Opt. Exp.*, vol. 19, no. 17, pp. 16697–16707, Aug. 2011. [Online]. Available: https://opg.optica.org/oe/abstract.cfm?URI=oe-19-17-16697